
Since January 2020 Elsevier has created a COVID-19 resource centre with free information in English and Mandarin on the novel coronavirus COVID-19. The COVID-19 resource centre is hosted on Elsevier Connect, the company's public news and information website.

Elsevier hereby grants permission to make all its COVID-19-related research that is available on the COVID-19 resource centre - including this research content - immediately available in PubMed Central and other publicly funded repositories, such as the WHO COVID database with rights for unrestricted research re-use and analyses in any form or by any means with acknowledgement of the original source. These permissions are granted for free by Elsevier for as long as the COVID-19 resource centre remains active.

Antiviral Research 144 (2017) 330–339

Contents lists available at ScienceDirect

Antiviral Research

journal homepage: www.elsevier.com/locate/antiviral

# Toward the identification of viral cap-methyltransferase inhibitors by fluorescence screening assay

Wahiba Aouadi [a, 1], Cécilia Eydoux [a, 1], Bruno Coutard [a], Baptiste Martin [a], Françoise Debart [b], Jean Jacques Vasseur [b], Jean Marie Contreras [c], Christophe Morice [c], Gilles Quérat [d], Marie-Louise Jung [c], Bruno Canard [a], Jean-Claude Guillemot [a, 1], Etienne Decroly [a, *, 1]

[a] Aix Marseille Université, CNRS, AFMB UMR 7257, Marseille, France
[b] IBMM, CNRS, Université Montpellier, ENSCM, Campus Triolet, Place E. Bataillon, 34095, Montpellier Cedex 05, France
[c] Prestwick Chemical, 67400, Illkirch, Strasbourg, France
[d] UMR "Emergence des Pathologies Virales" (EPV: Aix-Marseille Université - IRD 190 - Inserm 1207 - EHESP), Marseille, France

ARTICLE INFO

*Article history:*
Received 22 May 2017
Received in revised form
28 June 2017
Accepted 29 June 2017
Available online 1 July 2017

*Keywords:*
Methyltransferase
Coronavirus
Flavivirus
Inhibitor
HTRF
Antiviral

ABSTRACT

Two highly pathogenic human coronaviruses associated with severe respiratory syndromes emerged since the beginning of the century. The severe acute respiratory syndrome SARS-coronavirus (CoV) spread first in southern China in 2003 with about 8000 infected cases in few months. Then in 2012, the Middle East respiratory syndrome (MERS-CoV) emerged from the Arabian Peninsula giving a still ongoing epidemic associated to a high fatality rate. CoVs are thus considered a major health threat. This is especially true as no vaccine nor specific therapeutic are available against either SARS- or MERS-CoV. Therefore, new drugs need to be identified in order to develop antiviral treatments limiting CoV replication. In this study, we focus on the nsp14 protein, which plays a key role in virus replication as it methylates the RNA cap structure at the N7 position of the guanine. We developed a high-throughput N7-MTase assay based on Homogenous Time Resolved Fluorescence (HTRF®) and screened chemical libraries (2000 compounds) on the SARS-CoV nsp14. 20 compounds inhibiting the SARS-CoV nsp14 were further evaluated by $IC_{50}$ determination and their specificity was assessed toward flavivirus- and human cap N7-MTases. Our results reveal three classes of compounds: 1) molecules inhibiting several MTases as well as the dengue virus polymerase activity unspecifically, 2) pan MTases inhibitors targeting both viral and cellular MTases, and 3) inhibitors targeting one viral MTase more specifically showing however activity against the human cap N7-MTase. These compounds provide a first basis towards the development of more specific inhibitors of viral methyltransferases.

© 2017 Published by Elsevier B.V.

## 1. Introduction

The severe acute respiratory syndrome coronavirus (SARS-CoV) spread in China in 2003 and was responsible for worldwide outbreak causing over 8000 infected people with a fatality rate around 10% (de Wit et al., 2016). In 2012, a novel human coronavirus named Middle East Respiratory Syndrome Coronavirus (MERS-CoV) emerged in the Arabian Peninsula with secondary infection cases reported in Europe, America, Asia and Africa. MERS-CoV infection resulted in more than 1728 confirmed infected patients till April 2016 with a fatality rate of 36% (de Wit et al., 2016).

CoVs are enveloped viruses possessing a single stranded positive sense RNA genome of approximately 29.7 kb in length (Pan et al., 2008; Van Boheemen et al., 2012). The SARS-CoV initiates its replication cycle after binding to the angiotensin-converting enzyme 2 (ACE2) (Kuhn et al., 2004). After endocytosis, the viral RNA genome is released into the cellular host cytoplasm and translated into two large polyproteins (de Wit et al., 2016; Snijder et al., 2016). The pp1a and pp1ab polyproteins are next cleaved by viral proteases into 11 and 16 non-structural proteins respectively (nsp1 to 16). These proteins form a large replication transcription complex (RTC) which is associated to host cellular

* Corresponding author.
*E-mail address:* etienne.decroly@afmb.univ-mrs.fr (E. Decroly).
[1] These authors contributed equally to this work.

http://dx.doi.org/10.1016/j.antiviral.2017.06.021
0166-3542/© 2017 Published by Elsevier B.V.

proteins (Van Hemert et al., 2008). CoV RTC ensures the replication of the viral genome and the transcription of genomic and subgenomic mRNA. These viral RNAs are polyadenylated at their 3′ end and protected by a 5′ cap structure, which is synthetized by viral enzymes. The CoV capping pathway is thought to follow four sequential steps implicating several nsps: I) the 5′-3′ helicase/NTPase nsp13 hydrolyses first the phosphate γ from the nascent 5'-triphosphorylated RNA (Ivanov and Ziebuhr, 2004); II) a GMP molecule is supposedly transferred to the diphosphorylated RNA by a still unknown guanylyltransferase forming a cap (GpppN) structure; III) the cap is then methylated at N7 position of the guanosine by nsp14 in the presence of methyl donor S-adenosyl-L-methionine (SAM) yielding to a cap-0 ($^{7m}$GpppN) and S-adenosyl-L-homocysteine (SAH) by-product (Chen et al., 2009); IV) nsp10/nsp16 complex methylates at the ribose 2′OH group of the first transcribed RNA leading to the conversion of the cap-0 ($^{7m}$GpppN) into the cap-1 ($^{7m}$GpppN$_{2'om}$) (Bouvet et al., 2010; Chen et al., 2011). *In vitro* assays have deciphered the mechanisms driving the RNA cap methylation in SARS- and MERS-CoV. It follows an obligatory order in which N7-methylation by nsp14 is a pre-requisite for 2′O-methylation by the nsp10/nsp16 complex (Aouadi et al., 2017; Bouvet et al., 2014, 2010).

The guanine N7-MTase activity embedded in the C-terminal domain of SARS-nsp14 has been discovered by yeast trans-complementation assay (Chen et al., 2009). In addition, the N-terminus moiety of nsp14 contains a DEDDh exonuclease (ExoN) domain (Minskaia et al., 2006). The two domains communicate functionally, as truncation experiments showed that the N-terminal region of nsp14 is required for the N7-MTase activity (Chen et al., 2009). Both N7-MTase and ExoN activities have been confirmed by *in vitro* assay showing that the association of nsp10 to nsp14 stimulated >35 fold the ExoN activity while the N7-MTase activity does not depend on the nsp10-nsp14 interaction (Bouvet et al., 2012, 2010; Decroly et al., 2011).

The N7- and 2′O- methylations of the viral mRNA cap are key events for the viral infection. Indeed reverse genetic experiments revealed first that the N7- methylation of cap structures is essential for the synthesis of viral proteins (Case et al., 2016). This observation is corroborated by former biochemical data showing that the N7-methyl guanosine of cap structures is recognized by the eukaryotic translation initiation factor 4E (eIF4E) and participates in the initiation of viral mRNA translation into proteins (Case et al., 2016; Cougot et al., 2004). Accordingly, inhibitors blocking nsp14 N7-MTase activity have been identified by yeast based screening assay on SARS-CoV, and induced a potent antiviral effect demonstrating that nsp14 MTase activity is an attractive antiviral target (Sun et al., 2014). Whereas N7-MTase mutants are replication defective, 2′O-MTase mutants show limited effect on virus replication in cell culture but have an attenuated phenotype in animal models (Li et al., 2013; Menachery et al., 2014; Zhang et al., 2014; Züst et al., 2013). The molecular basis of this attenuated phenotype was recently elucidated: incompletely-capped RNAs have been shown to be recognized by immune sensors such as RIG-I and MDA-5, which trigger innate immunity pathways (Decroly et al., 2012; Schuberth-Wagner et al., 2015; Wu et al., 2013). In turn, RIG-I or MDA-5 induces signalling cascades yielding to the expression of cytokines and type I interferon inducing an antiviral state in neighboring cells. Among the interferon-stimulated gens (ISG), IFIT1 also participates to the restriction of viral replication by sequestrating mis-capped viral RNAs (Pichlmair et al., 2011). Thus cap structure is now considered as a kind of "marker of self" and it is currently admitted that 2′O-MTase inhibitors might help virus clearance by stimulation of the immune response (Decroly et al., 2012; Ferron et al., 2012; Züst et al., 2011).

In this work we first developed an HTRF MTase assay in order to identify compounds inhibiting the N7-MTase activity of SARS-CoV nsp14. Using this system, we screened a library composed of 2000 compounds containing 1280 FDA approved molecules (Prestwick Chemical Library®), 320 natural products and 400 pyridazine-derived compounds. The inhibitory effect of the 20 best compounds was confirmed by a radioactive filter-binding assay, and refined by $IC_{50}$ values determination on SARS nsp14 and human RNA N7-MTase (hRNMT). In addition, the specificity of each compound was further evaluated using the CoV 2′O-MTase (nsp10/nsp16) and the MTases of Dengue and West-Nile flaviviruses as well as the hRNMT involved in the capping of cellular RNAs.

## 2. Materials and methods

### 2.1. Description of the libraries

The Prestwick Chemical Library® is a unique collection of 1280 small molecules, mostly approved drugs (FDA, EMA and other agencies) selected for their high chemical and pharmacological diversity as well as for their known bioavailability and safety in humans. The Prestwick Phytochemical Library is a collection of 320 natural products, mostly derived from plants, assembled by medicinal chemists and rich in diverse chemotypes, thus realistic for follow-up chemistry. The Prestwick Pyridazine Library is a collection of 400 innovative pyridazine and pyridazone derivatives, based on a series of carefully selected new original scaffolds. All molecules have been designed to ensure optimal diversity, and are suitable for diverse chemical modification.

### 2.2. Expression and purification of recombinant proteins

The viral MTases (SARS-CoV nsp14, MERS-CoV nsp14, DENV-3 NS5-MTase, West Nile virus NS5-MTase, DENV-2 NS5-RdRp and human RNA N7-methyltransferase (RNMT) coding sequences were cloned in fusion with a N-terminus hexa-histidine tag in Gateway® plasmids (pDest14 or pDest17, Life technologies). The proteins were expressed in *E. coli* cells and purified following previously described protocols (Aouadi et al., 2017; Bouvet et al., 2010; Ma et al., 2015; Milhas et al., 2016; Peyrane et al., 2007; Selisko et al., 2006). MERS-CoV nsp14 was produced and purified as follows: the protein were expressed in Arctic Express *E. coli* strain (Agilent) at 13 °C during 24 h after addition of 50 μM IPTG. The bacteria were pelleted (13,000× g, 4 °C, 5 min), and lysed by sonication in appropriate buffer (50 mM Tris-HCl (pH 7.5), 150 mM NaCl, 5% glycerol, 20 mM imidazole, 5 mM β-mercaptoethanol, 1 mM PMSF, 10 μg/ml DNase-I and 0.25 mg/ml lysozyme). After clarification (50,000× g, 30 min at 4 °C) the recombinant protein was purified by immobilized metal affinity chromatography (IMAC) on 1 ml of HisPurTM Cobalt Resin (Thermo Scientific) followed by size exclusion chromatography on a Superdex 200 (GE healthcare) equilibrated in (30 mM HEPES pH (7.5), 300 mM NaCl and 5% glycerol). The purified proteins were analyzed on SDS-PAGE gels after Coomassie blue staining (Fig. 1 and Fig. S1).

### 2.3. HTRF screen on SARS CoV nsp14 MTase

For the initial screening, 400 nl of each compound resuspended in 100% DMSO at 1 mM were dispensed in the reaction volume (5% final DMSO, 50 μM compound) using a Mosquito Crystal pipetting robot platform (TTP labtech). DMSO, sinefungin (20 μM) and SAH (2 μM) were used as controls.

The enzymatic reaction was performed in 8 μl. 3 μl of mix (Buffer + SARS nsp14 at 5 nM final concentration) were added in the assay wells, containing previously dispensed inhibitors (0.4 μl), using a Biomek NX MC pipetting robot (Beckman). The reaction

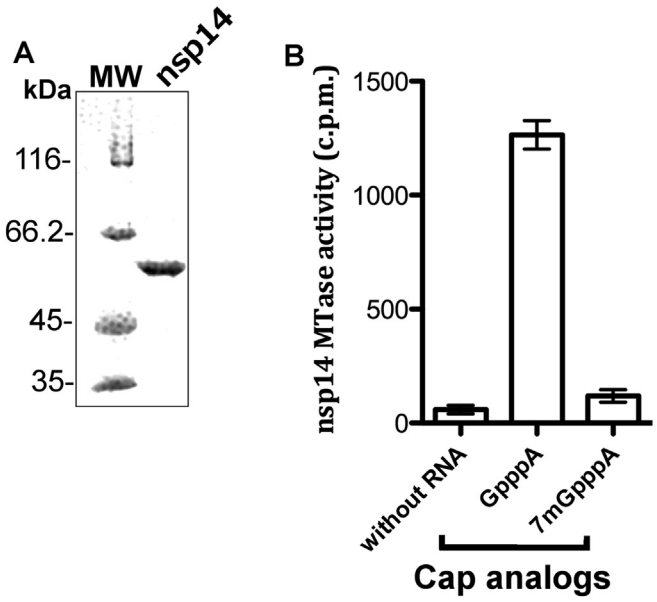


**Fig. 1. Characterization of the recombinant SARS-CoV nsp14**. A) 2.5 μg of SARS-CoV nsp14 on a 10% SDS-PAGE gel stained by Coomassie blue. MW, molecular size markers. B) Bar graph representing the N7-MTase activity of SARS-nsp14 determined by monitoring the transfer of tritiated methyl from [$^3$H] SAM onto GpppA and $^{7m}$GpppA. The tritiated RNA was quantified by DEAE filter binding assay (FBA).

buffer is composed of (Tris-HCl 40 mM (pH 8.0) and DTT 0.5 mM final concentrations). Reaction was started with 4.6 μl of a mix containing both GpppA (NEB ref S1406) and SAM at 8 μM and 2 μM final concentrations respectively and was incubated 20 min at 30 °C.

For the detection of released SAH, the EPIgeneous™ methyltransferase kit was purchased from CisBio Bioassays and reconstituted according to the supplier protocols. HTRF assays were performed in white 384 Well Small Volume™ HiBase Polystyrene Microplates (Greiner) with a final volume of 20 μl. 2 μl of EPIgeneous detection buffer one and 2 μl of NaCl 5 M were then added in order to stop the reaction. After 10 min of incubation at room temperature, detection reagents were added: 4 μl of a 1/16 dilution of SAH conjugated to the florescent dye d2 in a first place then 4 μl of Anti-SAH antibody-Lumi4-Tb at a 1/150 dilution. HTRF signals were measured, after a 1 h final incubation at room temperature, using a PHERAstar*FS* (BMG Labtech) with an excitation filter at 337 nm and fluorescence wavelength measurements at 620 and 665 nm, an integration delay of 60 μs and an integration time of 400 μs. Results were analyzed with a two-wavelength signal ratio: [intensity (665 nm)/intensity (620 nm)]*$10^4$ (HTRF Ratio). The normalized HTRF ratio is calculated as follow: [(compound signal) - (min signal)]/[(max signal) - (min signal)] * 100, where 'max signal' is the signal ratio without protein and 'min signal' the signal ratio with DMSO in place of compound.

The Z′ factor is calculated using the following equation: $Z' = 1 - [3(SD\ of\ max) + 3(SD\ of\ min)]/[(mean\ max\ signal) - (mean\ min\ signal)]$, where SD is the standard deviation. For $IC_{50}$ measurements, values were normalized and fitted with Prism (GraphPad software) using the following equation: Y = 100/(1 + ((X/IC50)^Hill slope)).

The initial screening assay was performed once and the hits were then confirmed by determination of $IC_{50\ (HTRF)}$ in quadruplicates. $IC_{50\ (HTRF)}$ is defined as the compound concentration for which the SAH release is decreased by 50%.

### 2.4. MTase filter binding assay (FBA)

The inhibitor specificity assays were carried out in reaction mixture [40 mM Tris-HCl (pH 8.0), 1 mM DTT, 1 mM $MgCl_2$, 2 μM SAM, and 0.33 μM $^3$H-SAM (Perkin Elmer)] in the presence of 0.7 μM $GpppAC_4$ or $^{7m}GpppAC_4$ synthetic RNAs. Purified SARS-nsp14 (10 nM), MERS-nsp14 (250 nM), SARS-nsp10/nsp16 (1 μM), MERS-nsp10/nsp16 (500 nM), hRNMT (20 nM), DENV-MT (500 nM) and WNV NS5 (500 nM). The enzymes were mixed first with 50 μM inhibitors before the addition of RNA substrate and SAM and then incubated at 30 °C. The final concentration of DMSO was 5%, and control reactions were performed in the presence of 5% DMSO.

Reaction mixtures were stopped after 30 min by their 10-fold dilution in ice-cold 100 μM SAH. Samples were transferred to Diethylaminoethyl cellulose filters (DEAE) (Perkin Elmer) using a Filtermat Harvester apparatus (Packard Instruments). The unincorporated $^3$H SAM was removed from the filter by several washing with 0.01 M ammonium formate pH (8.0), $H_2O$, then absolute ethanol, before drying of the DEAE filters. The filters were incubated with BetaplateScint (Wallac) scintillation fluid before quantification of $^3$H methylation transferred onto RNA substrates using a Wallac 1450 MicroBetaTriLux liquid scintillation counter in counts per minute (cpm).

The inhibition specificity of DV-2 RdRp was performed using 100 nM enzyme, 200 μM ATP, 4 μM [$^3$H] ATP and 100 nM polyU substrate into the buffer reaction [50 mM HEPES, 10 mM DTT, 5 mM $MgCl_2$, 2 mM $MnCl_2$]. The reaction was incubated during 10 min at 30 °C then stopped by adding 100 mM EDTA final concentration. The reaction mixture was then transferred onto DEAE filter as described above. The unincorporated [$^3$H]ATP during the RNA synthesis was removed from the filter with 0.2 M ammonium formate as described above. The $IC_{50}$ values of inhibitors on SARS-nsp14 and RNMT were determined using 0.35 μM GpppAUAU RNA mimicking the 5′ extremity of SARS-CoV genome and 0.35 μM $GpppAC_4$ for hRNMT. The $IC_{50}$ values were fitted as described above.

## 3. Results

### 3.1. Expression of active SARS-CoV nsp14 N7 MTase

SARS-CoV encodes the bi-functional enzyme nsp14, which contains an N-terminal ExoN domain followed by a N7-MTase domain involved in RNA capping. The recombinant protein was purified by immobilized metal affinity chromatography (IMAC) followed by size exclusion chromatography. The purified nsp14 is detected as a single band migrating at the expected molecular mass (Fig. 1A, ≈60 kDa) on Coomassie blue stained SDS-PAGE gels. The purified nsp14 transfers [$^3$H] methyl onto a GpppA cap analogue whereas no MTase activity is detected onto $^{7m}$GpppA (Fig. 1B) indicating that nsp14 harbors an N7-MTase activity that can be detected using cost effective commercial cap analogues.

### 3.2. Optimization of HTRF assay for high-throughput screening

We miniaturized the EPIgenous MTase assay based on Homogenous Time Resolved Fluorescence (HTRF) (Degorce et al., 2009) to screen a library of 2000 compounds. The principle of the HTRF assay, shown in Fig. S2, is to follow the MTase activity by indirectly detecting SAH, the by-product of the methyl transfer reaction. Indeed, in the detection system, the released SAH competes with fluorescent SAH-d2, which binds to an anti-SAH antibody coupled to a cryptate fluorophore (see Material and Methods). Thus, increase of SAH leads to decrease of the HTRF signal (Fig. S3D). The experimental conditions for the enzymatic assay were optimized

and adapted for automated screening assay. Briefly, I) the enzyme concentration was set up at 5 nM of nsp14 as titration curves indicated that 80% of the maximal activity after 20 min incubation period is obtained at this enzyme concentration (Fig. S3A); II) GpppA substrate concentration was adjusted at 8 μM to robustly and reproducibly detect N7-MTase activity (Fig. S3B); III) SAM concentration was adjusted to 2 μM in order to ensure the optimal conversion rate of SAM to SAH according to the manufacture recommendations (≈4–11%, Fig. S3C/D). The SAH detection conditions were optimized and the SAH-d2 and anti-SAH antibody were diluted 1/16 and 1/150 respectively.

Fig. 2A shows the time course experiment of nsp14 MTase activity indicating that using our experimental optimized conditions the N7-methylation reaction reached the saturation phase after a 30 min incubation period. The enzymatic reactions were thus incubated during 20 min in the screening. Sinefungin, which has already been reported to inhibit the SARS-CoV N7-MTase ($IC_{50}$ ≈ 500 nM) (Bouvet et al., 2010), was used as positive control for MTase inhibition. The inhibition curve of nsp14 MTase using the optimized HTRF assay revealed an inhibition in a similar range, with $IC_{50\ (HTRF)}$ value of 110 nM (Fig. 2B). We also assessed that the addition of DMSO up to 5% did not impact the MTase reactions and/or the HTRF quantification of released SAH. The signal variation was estimated to 2–2.8%. The average of Z′ value was 0.69.

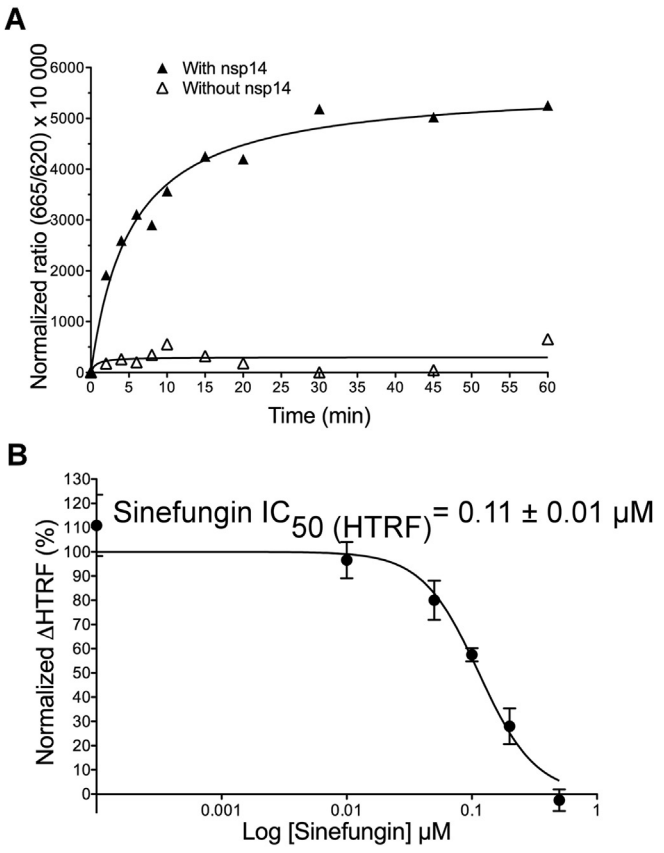


**Fig. 2. HTRF assay validation using SARS-nsp14**. A) Time course analysis of SARS-CoV nsp14 MTase activity by HTRF assay: 0 or 5 nM of nsp14 (empty or full triangles, respectively) are incubated with 8 μM GpppA and 2 μM SAM at 30 °C for increasing time periods. The reaction by-product (SAH) was quantified by measuring the ratio of emission and excitation fluorescence at 665 and 620 nm, on a PolarStar reader as described in materials and methods. B) Sinefungin $IC_{50\ (HTRF)}$ determination. Increasing concentrations of sinefungin (0–0.5 μM) were incubated with 5 nM nsp14, 2 μM SAM, 8 μM GpppA at 30 °C during 20 min and the SAH by-product was detected as described in panel A. The $IC_{50\ (HTRF)}$ was then calculated using graphPad Prism equation (n = 3; Mean value ± SD).

### 3.3. HTRF screening of inhibitors against SARS-CoV nsp14 N7-MTase activity

The chemical library containing 1280 FDA approved molecules, 320 natural substrates and 400 pyridazine derived compounds was used for initial screening at 50 μM of each compound and the inhibition was determined using HTRF assay. Compounds showing inhibition of the MTase activity higher than 42%, which corresponds to increase of the HTRF signal >20% (Fig. S4), were first selected (41 compounds, Fig. 3). 21 compounds were discarded due to signal interference with the HTRF assay or by visual inspection. The 20 remaining compounds (hit rate 0.1%, Table 1) were selected for $IC_{50\ (HTRF)}$ determination by HTRF. The results presented in Table 1 indicate that the $IC_{50\ (HTRF)}$ vary from 0.16 to > 400 μM, among which 4 have an $IC_{50\ (HTRF)}$ higher than 75μM. $IC_{50\ (HTRF)}$ for 1159, 597, 194 were not determined due to intrinsic fluorescence interferences at high concentration. Thus, 13 compounds show $IC_{50\ (HTRF)}$ ranging from 0.16 to 75 μM.

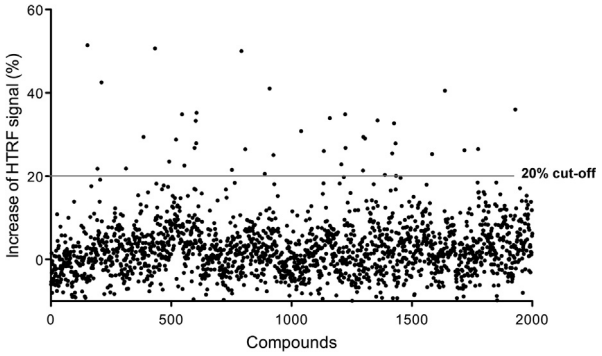


**Fig. 3. Distribution of inhibition percentage values obtained by HTRF screening on Prestwick Chemical libraries**. The 2000 compounds were screened at 50 μM, 5% DMSO on SARS CoV nsp14 MTase activity using HTRF assay (5 nM nsp14, 8 μM GpppA, 2 μM SAM, SAH-d2 (1/16) and anti-SAH (1/150)). The grey line corresponds to an increase of 20% of the HTRF signal that was used as a threshold for the selection of the primary hits.

**Table 1**
Screening results and $IC_{50\ (HTRF)}$ of selected compounds on the SARS-nsp14 by HTRF assay.

| Compounds | HTRF signal increase at 50 μM (%) | $IC_{50\ (HTRF)}$ (μM) |
|---|---|---|
| 152 | 51.4 | 171.5 ± 16 |
| 792 | 50 | 5.8 ± 2 |
| 210 | 42.5 | 17.1 ± 5.6 |
| 909 | 41 | >400 |
| 545 | 34.8 | >400 |
| 1159 | 33.9 | Not available |
| 602 | 33.3 | 73.6 ± 29 |
| 1426 | 32.7 | 0.16 ± 0.02 |
| 1040 | 30.8 | 5.5 ± 1 |
| 1298 | 29.4 | 2 ± 0.6 |
| 1305 | 29 | 3.3 ± 0.7 |
| 604 | 27.9 | 57.2 ± 15 |
| 597 | 26.8 | Not available |
| 1418 | 25.4 | 18.9 ± 3.8 |
| 925 | 25 | 5 ± 0.6 |
| 1207 | 22.8 | 73 ± 9.3 |
| 312 | 21.8 | 38.6 ± 5 |
| 194 | 21.8 | Not available |
| 752 | 21.5 | 35.5 ± 7.3 |
| 1434 | 20 | >400 |
| Sinefungin | 96.9 | 0.112 ± 0.01 |

Not available: $IC_{50\ (HTRF)}$ not accurate due to fluorescence issues at high compound concentrations.

### 3.4. Hit confirmation by radioactive MTase assay on SARS-CoV nsp14

In order to validate the inhibition observed by HTRF, we next performed a radioactive MTase assay (FBA) using freshly solubilized compounds. In this experiment, the MTase activity was analyzed by measuring the [$^3$H] radiolabeled methyl transferred onto a longer synthetic RNA substrate ($GpppAC_4$). This capped RNA was previously evidenced as a better substrate for nsp14 N7-MTase than the cap analogue GpppA (Bouvet et al., 2010). The low inhibition of the 4 compounds showing $IC_{50\ (HTRF)} > 75\ \mu M$ by HTRF (1434, 152, 545, 909), was confirmed by the FBA assay. In addition the fluorescent compounds 194, 597 poorly inhibits the MTase activity in this FBA assay. Finally, eleven compounds display a potent inhibition (>80%) at 50 μM concentration using the radioactive assay (Table 2). Whereas we observed some discrepancies between HTRF and FBA assay for a couple of compounds (210 and 909), which could be explained by the difference in RNA substrate length used in both assays; we observed a good correlation between both assays.

**Table 2**
Inhibition specificity of compounds at 50 μM on MTases and DENV-2 polymerase activities using DEAE-filter binding assay.

| Compounds | Inhibition percentage at 50 μM (%) | | | | | | | |
|---|---|---|---|---|---|---|---|---|
| | SARS nsp14 | MERS nsp14 | SARS nsp10/16 | MERS nsp10/16 | RNMT | DENV-MT | WNV NS5 | DV-2 Rdrp |
| Sinefungin | 98.4 | 73.5 | 98.4 | 77 | 98.2 | 98.3 | 98.4 | 11 |
| 925 | 96.9 | 94.2 | 88.3 | 98 | 96 | 98.9 | 98.5 | 99 |
| 1426 | 95.3 | 38.1 | 89.5 | 87.7 | 97 | 85 | 94.1 | 72 |
| 1298 | 93.6 | 46.2 | 64.9 | 76.8 | 97 | 44.9 | 48.2 | 98 |
| 1305 | 92.2 | 37.4 | 69.5 | 83.6 | 97.8 | 60.3 | 58.9 | 85 |
| 1159 | 83 | 50.8 | 72.5 | 8.2 | 94.7 | 37.6 | 30.2 | 72 |
| 1040 | 90.5 | 85.6 | 92.9 | 94.5 | 98.6 | 97.8 | 66.3 | 13 |
| 792 | 81.3 | 62 | 94 | 85.5 | 96.5 | 19.1 | 39.6 | 47 |
| 312 | 93.7 | 63.5 | 63.3 | 9.5 | 66.7 | 33 | 18.5 | 26 |
| 1418 | 85.9 | 24.4 | 33.2 | 57.5 | 82.7 | 30 | 32 | 44 |
| 1207 | 93.5 | 42.1 | 38.7 | 13.1 | 42.5 | 14.6 | 33.1 | 14 |
| 604 | 93.7 | 39.3 | 34.2 | 7.6 | 95 | 12.2 | 22.7 | 6 |
| 752 | 37.3 | 38.1 | 13.7 | 0 | 0 | 28.3 | 0 | 8 |
| 1434 | 36.4 | 34.9 | 20.3 | 0 | 0 | 37 | 0 | 13 |
| 602 | 24.34 | 33.5 | 1 | 0 | 0 | 25.8 | 0 | 4 |
| 194 | 22.3 | 4.9 | 31.6 | 0 | 0 | 32.6 | 12.8 | 8 |
| 152 | 19.8 | 16.7 | 6.8 | 13.7 | 6 | 3 | 23.7 | 0 |
| 597 | 10.9 | 0 | 0 | 0 | 0 | 4 | 15.7 | 4 |
| 545 | 8.5 | 36.9 | 0 | 0 | 0 | 9.4 | 11.5 | 11 |
| 909 | 7.3 | 13.1 | 13.4 | 5.9 | 0 | 2.4 | 9.6 | 0 |
| 210 | 0.63 | 27.4 | 36.1 | 12.7 | 88.6 | 15.4 | 32.2 | 14 |

The compounds are clustered and framed according to their inhibition specificity from wide range to specific inhibitors. ND: Not determined.

### 3.5. Assessment of the inhibitors specificity using other viral and cellular MTases

The specificity of the 20 compounds was then analyzed by measuring their inhibition profile on other viral and cellular MTases (for more details see workflow in Fig. S5). We thus produced and purified the SARS- and MERS-CoV nsp14 and the nsp10/nsp16 complex (2′O-MTase); the full length NS5 of the West Nile (WNV) and NS5-MTase domain of Dengue 3 (DENV-3) viruses and the human RNA N7-MTase (hRNMT) (Fig. S1) in order to compare their inhibition profile. The inhibition of each compound (50 μM) was then determined by FBA MTase activity measurements. In addition, we also tested whether the DENV-2-RdRp activity is inhibited in order to address the compound specificity. The results summarized in Table 2 show that among the 11 best SARS-CoV nsp14 inhibitors confirmed by FBA (Table 5), 5 (925, 1426, 1298, 1305, 1159) show large spectrum inhibition as they inhibit all tested MTases as well as the DENV-2 RdRp. Table 2 also reveals that sinefungin (used as positive control) and compound 1040 exhibit a broad spectrum MTase inhibition profile with no inhibition detected on the RdRp activity of DENV NS5. This broad-spectrum inhibition observed with sinefungin has already been reported and can be related to its structural homology with the SAM/SAH (Dong et al., 2010). Interestingly, compound 792 inhibits mainly the CoV N7- and 2′O-MTase as well as the hRNMT but barely interferes with DENV-3 or WNV NS5 MTase activity. Finally, the four last compounds (312, 1418, 1207, 604) show more specific inhibition profile on MERS- and SARS-CoV nsp14 although they inhibit the hRNMT.

To further characterize the eleven most potent nsp14 N7-MTase inhibitors, a dose response curve was performed with the compounds showing percentage inhibition higher or equal to 40% against SARS-CoV nsp14 and the hRNMT. After pre-incubation with increasing concentrations of inhibitors, the MTase activity was followed by FBA. The $IC_{50}$ of compounds on either nsp14 or hRNMT activities ranged from 19 nM to 23 μM and 50 nM to 5.5 μM, respectively, confirming the observed inhibition potency of these molecules (Table 3). In addition, the $IC_{50}$ values determined in this assay corroborate with those performed by HTRF assay (Table 1). The broad spectrum MTase inhibitor (1040) shows $IC_{50}$ values of 4.5 and 5.1 μM on SARS nsp14 and human hRNMT respectively and four compounds targeting more specifically SARS, MERS and hRNMT have $IC_{50}$ values between 10 and 24 μM, but $IC_{50}$ values observed with for hRNMT are lower in each case.

Altogether these results suggest that structural homology between viral and cellular MTases might impair the discovery of inhibitors targeting specifically the CoV N7-MTase (see discussion about homology). Nevertheless, we also observed that the less active inhibitors on SARS-CoV nsp14 barely inhibit the human hRNMT suggesting the possibility to identify more specific MTase inhibitors (Table 2). A structure activity relationship (SAR) study is required in order to gain in activity and specificity.

**Table 3**
Comparison of the $IC_{50}$ value of 11 most active compounds on SARS-nsp14 and human RNMT activities using GpppAUAU and $GpppAC_4$ substrates respectively.

| Compounds | $IC_{50}$ SARS-nsp14 (μM) | $IC_{50}$ RNMT (μM) |
|---|---|---|
| Sinefungin | 0.36 ± 0.08 | <0.05 |
| 925 | 1.5 ± 0.11 | 1 ± 0.1 |
| 1426 | 0.019 | ND |
| 1298 | 0.74 ± 0.1 | 0.32 ± 0,27 |
| 1305 | 1.3 ± 0.2 | 0.4 ± 0.05 |
| 1040 | 4.5 ± 0.35 | 5.1 ± 2.28 |
| 792 | 31 ± 3 | 5.5 ± 1.92 |
| 1159 | 2 ± 0.44 | <0.05 |
| 312 | 12.3 ± 1 | 4.84 ± 1.6 |
| 1418 | 23.7 ± 7 | 10 ± 3 |
| 1207 | 18.4 ± 2 | ND |
| 604 | 11 ± 1 | 1.28 ± 0.16 |

ND: Not Determined.

### 3.6. Inhibition of SARS-CoV nsp14 by compound 312 analogs already present in the library

Following the confirmation of compound 312, analogs were

**Table 4**
Evaluation of compound 312 analogs. $IC_{50}$ determined by FBA on SARS-CoV nsp14 and RNMT MTase activities using $GpppAC_4$ substrate.

| Compounds | Structure | $IC_{50}$ (μM) on | |
|---|---|---|---|
| | | SARS nsp14 | RNMT |
| 312 | 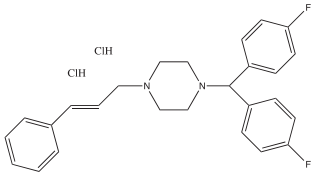 | 7.3 ± 0.4 | 14.3 ± 1 |
| 457 | 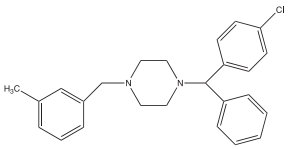 | 6.2 ± 0.4 | 8.8 ± 0.6 |
| 278 | 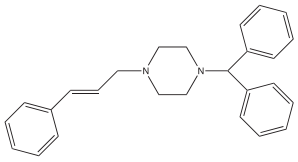 | 9.1 ± 0.7 | 16.8 ± 2 |
| 1264 | 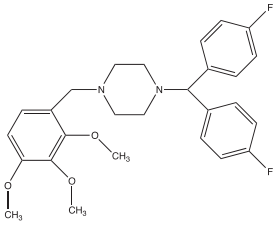 | 13.5 ± 2 | 13.7 ± 0.8 |
| 133 | 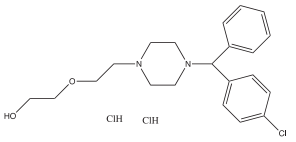 | No inhibition | 365.2 ± 186 |
| 510 | 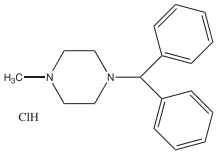 | No inhibition | 159 ± 36 |
| 706 | 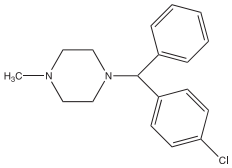 | No inhibition | 226.8 ± 29 |
| 503 | 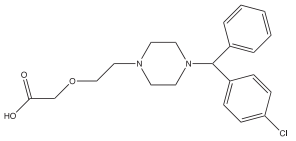 | No inhibition | 102.2 ± 21 |

**Table 5**
Structure of the most active compounds.

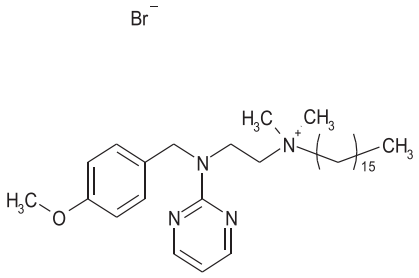

Compound 925

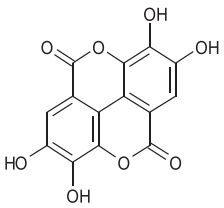

Compound 1426

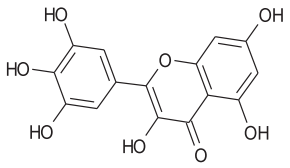

Compound 1298

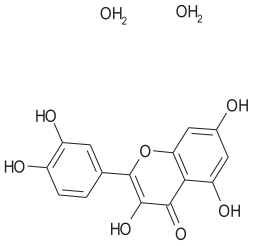

Compound 1305

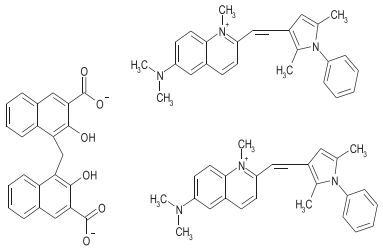

Compound 1040

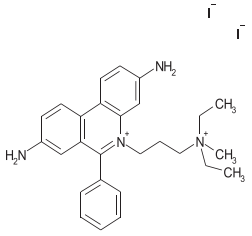

Compound 792

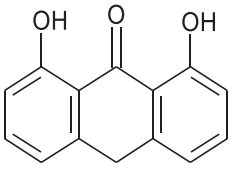

Compound 1159

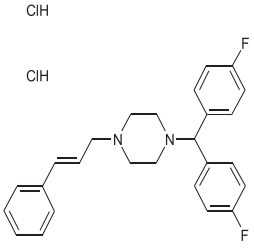

Compound 312

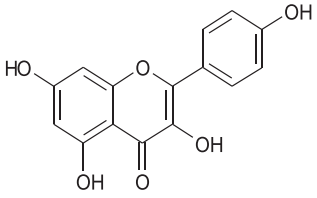

Compound 1418

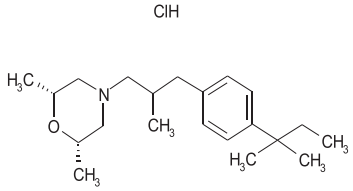

Compound 1207

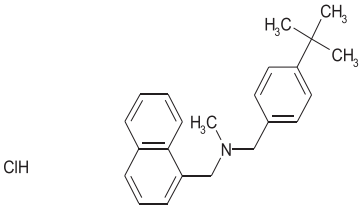

Compound 604

searched in the tested libraries. 7 analogs were selected and tested for inhibition of SARS nsp14 and hRNMT MTase activities by FBA (Table 4). All the 7 analogs bear the benzhydryl-piperazine group characteristic to this chemical series in the right-hand side of the structure. Four compounds lacking the aromatic moiety in the left part of the molecule show no inhibition of SARS-CoV nsp14 MTase. In contrast, 3 analogs carrying an aromatic terminal ring in the left-hand side inhibit the SARS-CoV N7-MTase activity with $IC_{50}$ between 6.2 and 14 μM (457, 278 and 1264). The substitution of the two phenyl rings in the benzhydryl-piperazine moiety (fluorine or chlorine groups) have no impact on the inhibition profile. These compounds were initially not selected from the original screening but their inhibition was close to the selection cut-off (42% inhibition at 50 μM). The compounds inhibited the hRNMT and SARS-CoV nsp14 to similar levels. Although they did not bring additional specificity compared to compound 312, it might be worth sampling a larger chemical space within this family.

## 4. Discussion

The identification of molecules inhibiting viral enzymes essential for virus replication is a key point to combat emerging viruses. Methylations of viral mRNA cap structures are an essential step in the virus life-cycle (Case et al., 2016; Cougot et al., 2004) preventing their identification as foreign RNA markers by the host cell (Diamond, 2014; Li et al., 2013; Züst et al., 2013). Thus, enzymes such as MTases involved in viral RNA capping are now considered as promising antiviral targets (Ferron et al., 2012). Here, we developed a high-throughput MTase screening assay based on HTRF technology that possesses advantageous features. The HTRF assay allows the minimization of non-specific fluorescence emissions by introducing a time delay (50–150 μs) between the initial light excitation and fluorescence measurement (Degorce et al., 2009). This time delay limits the interference of fluorescent compounds in the screening assay. Indeed, only 37 out of 2000 compounds interfered with the detection system among which were considered as 17 false positive. In addition, a non-fluorescent enzymatic assay (FBA) was used to confirm the hits obtained from the primary screening. The initial screening was performed using a commercial cap analogue substrate (GpppA), as the availability of high amount of capped RNA substrates is a limiting step. This screening allowed the identification of 20 compounds inhibiting at least 42% of the nsp14 N7-MTase activity. The inhibitory effect (below 25 μM, Table 3) of 11 of these compounds was confirmed using a radioactive filter-binding assay performed with longer synthetic RNA substrates ($GpppAC_4$). In contrast, 9 compounds barely inhibited the MTase activity measured with $GpppAC_4$ substrate. Thus, it is likely that the use of GpppA as substrate may favor the identification of inhibitors that would be less efficient on longer RNA substrates. The weaker inhibition effect observed using longer RNA substrates might suggest that these compounds interfere with the RNA binding site of the enzyme.

One important issue in the drug discovery process is to identify compounds inhibiting specifically the viral enzymes but barely active on the cognate cellular enzymes in order to limit their cytotoxicity or off-target effects. To determine the compound specificity at the early stage of the screening process, we compared the inhibition activity of the 20 compounds on other viral MTases (SARS- and MERS-CoV 2′O MTase, DEN-V and WNV N7/2′O MTases) and a cellular MTase hRNMT involved in the methylation of cap structures. In addition, we also tested these compounds on the Dengue virus polymerase in order to control the inhibition specificity on the RdRp activity and eliminate molecules showing unspecific inhibition or frequent hitters. This strategy revealed that 5 out of the 11 best hits identified in the nsp14 N7-MTase activity-screening campaign potently inhibited all MTases tested as well as the Dengue virus polymerase.

We also observed that most inhibitors identified in this comparative screening potently inhibit the human RNA N7-MTase hRNMT (12 over 20 compounds). These results might be related to structural and functional homologies between CoV N7-MTase and the human hRNMT limiting the possibility to identify inhibitors targeting specifically the CoV N7-MTase. However, we would like to propose that the inhibitors identified here might well be substrate mimicks and bind to conserved substrate pockets since the protein folding of hRNMT and nsp14 are significantly different, the latter deviating from classical Rossman-fold MTases. It is also noteworthy that this work was performed with a highly active truncated construct of hRNMT, which is used at very low concentration (20 nM) for $IC_{50}$ determination. Additionally, it is also possible that as our truncated hRNMT is less selective as it lacks the hRNMT activating Miniprotein (RAM) binding domain and the RAM protein. Indeed it was previously demonstrated that RAM stabilizes the structure and positioning of the hRNMT lobe and increases the specific recruitment of SAM (Varshney et al., 2016). This high inhibition of hRNMT MTase activity may be overcome in the presence of its allosteric activator RAM, which may allow to stringent the specificity of the compounds.

Out of nsp14, the comparative screening using various MTases also reveals that several compounds show a large spectrum of MTase inhibition without any significant activity detected on the Dengue virus polymerase used as a control (compounds 1040 and the positive control sinefungin). The pleiotropic inhibition observed on MTases activities suggests that despite the weak primary sequence conservation, these enzymes do have a common structural organization (Rosmann fold characteristic of most of viral and cellular MTases) and share similar enzymatic properties. This observation is consistent with the common structural organization, with a conserved SAM, RNA and/or cap binding sites, shared by those MTases. The identification of broad-spectrum viral MTases inhibitors may offer a starting point to develop new antiviral compounds. We considered that these molecules could be interesting as we expected that the SAR process will give the opportunity to increase both specificity and inhibition properties. Accordingly, a SAR study previously performed on the flavivirus MTases has demonstrated that chemical analogs of SAH, showed improved activity and selectivity against DENV MTase, but not on the related human enzymes (Lim et al., 2011). The crystal structure revealed that the most active SAH derivative harbors substitutions accommodated in a specific cavity conserved in Flaviviral MTases. It would be thus relevant to initiate the structural analysis of viral MTases in complex with the best compounds in order to improve selectivity.

## 5. Conclusion

Viral N7- and 2′O-MTase is now considered as promising antiviral target as their inhibition is supposed to impair mRNA translation into viral proteins and to induce the stimulation of the innate immune system of the infected host. Thus it is currently accepted that MTase inhibitors might help virus clearance by stimulation of the immune response (Decroly et al., 2012; Ferron et al., 2012; Züst et al., 2011). In this work we identified 20 molecules inhibiting the N7-MTase activity of SARS-CoV nsp14 from chemical libraries composed of 2000 compounds using an HTRF based inhibition assay. Eleven compounds demonstrated a potent inhibition (>80%) at 50 μM concentration using the radioactive assay. The specificity of each compound was further evaluated using a radioactive assay on CoV 2′O-MTase (nsp10/nsp16) and the MTases of Dengue and West-Nile viruses as well as the human RNA N7-MTase (hRNMT)

involved in the capping of cellular RNAs. This comparative analysis revealed that the selected compounds cluster in 3 classes: 1) barely specific inhibitors, 2) pan-MTases inhibitors inhibiting viral and cellular MTases, 3) inhibitors targeting more specifically one viral MTase but also active against the hRNMT. These latter series of inhibitors may represent a good starting point for the development of antivirals targeting the CoV MTases.

## Acknowledgments

We are grateful to Eric Trinquet and Thomas Roux for helpful discussions on the HTRFassay. We thank Alexandre Blanjoie for HPLC purification of high amount of $GpppAC_4$ substrates.

This work was supported by the French research agency ANR [VMTaseIn, grant ANR-ST14-ASTR-0026], and SARS-RNA-SPA, [grant ANR-12BSV3-0007] and the PACA regional fundings. BM is the recipient of a DGA-MRIS scholarship and WA the recipient of a scholarship from the "Méditerranée Infection" Foundation and Fondation pour la Recherche Médicale (FRM: FDT20160434967).

## Appendix A. Supplementary data

Supplementary data related to this article can be found at http://dx.doi.org/10.1016/j.antiviral.2017.06.021.

## References

Aouadi, W., Blanjoie, A., Vasseur, J., Canard, B., Decroly, E., 2017. Binding of the methyl donor S-Adenosyl-L-Methionine to Middle East respiratory syndrome coronavirus 2'-O- methyltransferase nsp16 promotes recruitment of the allosteric activator nsp10. J. Virol. 91, 1–18.

Bouvet, M., Debarnot, C., Imbert, I., Selisko, B., Snijder, E.J., Canard, B., Decroly, E., 2010. In vitro reconstitution of SARS-coronavirus mRNA cap methylation. PLoS Pathog. 6, e1000863. http://dx.doi.org/10.1371/journal.ppat.1000863.

Bouvet, M., Imbert, I., Subissi, L., Gluais, L., Canard, B., Decroly, E., 2012. RNA 3 '-end mismatch excision by the severe acute respiratory syndrome coronavirus nonstructural protein nsp10/nsp14 exoribonuclease complex. PNAS 109, 9372–9377. http://dx.doi.org/10.1073/pnas.1201130109/-/DCSupplemental. www.pnas.org/cgi/doi/10.1073/pnas.1201130109.

Bouvet, M., Lugari, A., Posthuma, C.C., Zevenhoven, J.C., Bernard, S., Betzi, S., Imbert, I., Canard, B., Guillemot, J.C., Lécine, P., Pfefferle, S., Drosten, C., Snijder, E.J., Decroly, E., Morelli, X., 2014. Coronavirus Nsp10, a critical co-factor for activation of multiple replicative enzymes. J. Biol. Chem. 289, 25783–25796. http://dx.doi.org/10.1074/jbc.M114.577353.

Case, J.B., Ashbrook, A.W., Dermody, T.S., Denison, M.R., 2016. Mutagenesis of S-Adenosyl-L-Methionine-Binding residues in coronavirus nsp14 N7-methyltransferase demonstrates differing requirements for genome translation and resistance to innate immunity. J. Virol. 90, 7248–7256. http://dx.doi.org/10.1128/JVI.00542-16.

Chen, Y., Cai, H., Pan, J., Xiang, N., Tien, P., Ahola, T., Guo, D., 2009. Functional screen reveals SARS coronavirus nonstructural protein nsp14 as a novel cap N7 methyltransferase. PNAS 106, 3484–3489. http://dx.doi.org/10.1073/pnas.0808790106.

Chen, Y., Su, C., Ke, M., Jin, X., Xu, L., Zhang, Z., Wu, A., Sun, Y., Yang, Z., Tien, P., Ahola, T., Liang, Y., Liu, X., Guo, D., 2011. Biochemical and structural insights into the mechanisms of SARS coronavirus RNA ribose 2′-O-methylation by nsp16/nsp10 protein complex. PLoS Pathog. 7, e1002294. http://dx.doi.org/10.1371/journal.ppat.1002294.

Cougot, N., Van Dijk, E., Babajko, S., Séraphin, B., 2004. Cap-tabolism. Trends Biochem. Sci. 29, 436–444. http://dx.doi.org/10.1016/j.tibs.2004.06.008.

de Wit, E., van Doremalen, N., Falzarano, D., Munster, V.J., 2016. SARS and MERS: recent insights into emerging coronaviruses. Nat. Rev. Microbiol. 14, 523–534. http://dx.doi.org/10.1038/nrmicro.2016.81.

Decroly, E., Debarnot, C., Ferron, F., Bouvet, M., Coutard, B., Imbert, I., Gluais, L., Papageorgiou, N., Sharff, A., Bricogne, G., Ortiz-Lombardia, M., Lescar, J., Canard, B., 2011. Crystal structure and functional analysis of the SARS-coronavirus RNA cap 2′-O-methyltransferase nsp10/nsp16 complex. PLoS Pathog. 7, e1002059. http://dx.doi.org/10.1371/journal.ppat.1002059.

Decroly, E., Ferron, F., Lescar, J., Canard, B., 2012. Conventional and unconventional mechanisms for capping viral mRNA. Nat. Rev. Microbiol. 10, 51–65. http://dx.doi.org/10.1038/nrmicro2675.

Degorce, F., Card, A., Soh, S., Trinquet, E., Knapik, G.P., Xie, B., 2009. HTRF: a technology tailored for drug discovery - a review of theoretical aspects and recent applications. Curr. Chem. Genomics 3, 22–32. http://dx.doi.org/10.2174/1875397300903010022.

Diamond, M.S., 2014. IFIT1: a dual sensor and effector molecule that detects non-2'-O methylated viral RNA and inhibits its translation. Cytokine Growth Factor Rev. 25, 543–550. http://dx.doi.org/10.1016/j.cytogfr.2014.05.002.

Dong, H., Liu, L., Zou, G., Zhao, Y., Li, Z., Lim, S.P., Shi, P.Y., Li, H., 2010. Structural and functional analyses of a conserved hydrophobic pocket of flavivirus methyltransferase. J. Biol. Chem. 285, 32586–32595. http://dx.doi.org/10.1074/jbc.M110.129197.

Ferron, F., Decroly, E., Selisko, B., Canard, B., 2012. The viral RNA capping machinery as a target for antiviral drugs. Antivir. Res. 96, 21–31. http://dx.doi.org/10.1016/j.antiviral.2012.07.007.

Ivanov, K.A., Ziebuhr, J., 2004. Human coronavirus 229E nonstructural protein 13: characterization of duplex-unwinding, nucleoside triphosphatase, and RNA 5'-triphosphatase activities. J. Virol. 78, 7833–7838. http://dx.doi.org/10.1128/JVI.78.14.7833-7838.2004.

Kuhn, J.H., Li, W., Choe, H., Farzan, M., 2004. Angiotensin-converting enzyme 2: a functional receptor for SARS coronavirus. Cell. Mol. Life Sci. 61, 2738–2743. http://dx.doi.org/10.1007/s00018-004-4242-5.

Li, S.-H., Dong, H., Li, X.-F., Xie, X., Zhao, H., Deng, Y.-Q., Wang, X.-Y., Ye, Q., Zhu, S.-Y., Wang, H.-J., Zhang, B., Leng, Q.-B., Zuest, R., Qin, E.-D., Qin, C.-F., Shi, P.-Y., 2013. Rational design of a flavivirus vaccine by abolishing viral RNA 2'-O methylation. J. Virol. 87, 5812–5819. http://dx.doi.org/10.1128/JVI.02806-12.

Lim, S.P., Sonntag, L.S., Noble, C., Nilar, S.H., Ng, R.H., Zou, G., Monaghan, P., Chung, K.Y., Dong, H., Liu, B., Bodenreider, C., Lee, G., Ding, M., Chan, W.L., Wang, G., Jian, Y.L., Chao, A.T., Lescar, J., Yin, Z., Vedananda, T.R., Keller, T.H., Shi, P.Y., 2011. Small molecule inhibitors that selectively block dengue virus methyltransferase. J. Biol. Chem. 286, 6233–6240. http://dx.doi.org/10.1074/jbc.M110.179184.

Ma, Y., Wu, L., Shaw, N., Gao, Y., Wang, J., Sun, Y., Lou, Z., Yan, L., Zhang, R., Rao, Z., 2015. Structural basis and functional analysis of the SARS coronavirus nsp14-nsp10 complex. PNAS 112, 9436–9441. http://dx.doi.org/10.1073/pnas.1508686112.

Menachery Jr., V.D., B.L.Y., Josset, L., Gralinski, L.E., Scobey, T., Agnihothram, S., Katze, M.G., Baric, R.S., 2014. Attenuation and restoration of severe acute respiratory syndrome coronavirus mutant lacking 2′-O-methyltransferase activity. J. Virol. 88, 4251–4264. http://dx.doi.org/10.1128/JVI.03571-13.

Milhas, S., Raux, B., Betzi, S., Derviaux, C., Roche, P., Restouin, A., Basse, M.J., Rebuffet, E., Lugari, A., Badol, M., Kashyap, R., Lissitzky, J.C., Eydoux, C., Hamon, V., Gourdel, M.E., Combes, S., Zimmermann, P., Aurrand-Lions, M., Roux, T., Rogers, C., M??ller, S., Knapp, S., Trinquet, E., Collette, Y., Guillemot, J.C., Morelli, X., 2016. Protein-protein interaction inhibition (2P2I)-oriented chemical library accelerates hit discovery. ACS Chem. Biol. 11, 2140–2148. http://dx.doi.org/10.1021/acschembio.6b00286.

Minskaia, E., Hertzig, T., Gorbalenya, A.E., Campanacci, V., Cambillau, C., Canard, B., Ziebuhr, J., 2006. Discovery of an RNA virus 3'->5' exoribonuclease that is critically involved in coronavirus RNA synthesis. PNAS 103, 5108–5113. http://dx.doi.org/10.1073/pnas.0508200103.

Pan, J., Peng, X., Gao, Y., Li, Z., Lu, X., Chen, Y., Ishaq, M., Liu, D., DeDiego, M.L., Enjuanes, L., Guo, D., 2008. Genome-wide analysis of protein-protein interactions and involvement of viral proteins in SARS-CoV replication. PLoS ONE 3. http://dx.doi.org/10.1371/journal.pone.0003299.

Peyrane, F., Selisko, B., Decroly, E., Vasseur, J.J., Benarroch, D., Canard, B., Alvarez, K., 2007. High-yield production of short GpppA- and 7MeGpppA-capped RNAs and HPLC-monitoring of methyltransfer reactions at the guanine-N7 and adenosine-2'O positions. Nucleic Acids Res. 35 http://dx.doi.org/10.1093/nar/gkl1119.

Pichlmair, A., Lassnig, C., Eberle, C.-A., Górna, M.W., Baumann, C.L., Burkard, T.R., Bürckstümmer, T., Stefanovic, A., Krieger, S., Bennett, K.L., Rülicke, T., Weber, F., Colinge, J., Müller, M., Superti-Furga, G., 2011. IFIT1 is an antiviral protein that recognizes 5′-triphosphate RNA. Nat. Immunol. 12, 624–630. http://dx.doi.org/10.1038/ni.2048.

Schuberth-Wagner, C., Ludwig, J., Bruder, A.K., Herzner, A.M., Zillinger, T., Goldeck, M., Schmidt, T., Schmid-Burgk, J.L., Kerber, R., Wolter, S., Stümpel, J.P., Roth, A., Bartok, E., Drosten, C., Coch, C., Hornung, V., Barchet, W., Kümmerer, B.M., Hartmann, G., Schlee, M., 2015. A conserved histidine in the RNA sensor RIG-I controls immune tolerance to N1-2'O-methylated self RNA. Immunity 43, 41–51. http://dx.doi.org/10.1016/j.immuni.2015.06.015.

Selisko, B., Dutartre, H., Guillemot, J.C., Debarnot, C., Benarroch, D., Khromykh, A., Desprès, P., Egloff, M.P., Canard, B., 2006. Comparative mechanistic studies of de novo RNA synthesis by flavivirus RNA-dependent RNA polymerases. Virology 351, 145–158. http://dx.doi.org/10.1016/j.virol.2006.03.026.

Snijder, E.J., Decroly, E., Ziebuhr, J., 2016. Chapter three – the nonstructural proteins directing coronavirus RNA synthesis and processing. In: Advances in Virus Research, pp. 59–126. http://dx.doi.org/10.1016/bs.aivir.2016.08.008.

Sun, Y., Wang, Z., Tao, J., Wang, Y., Wu, A., Yang, Z., Wang, K., Shi, L., Chen, Y., Guo, D., 2014. Yeast-based assays for the high-throughput screening of inhibitors of coronavirus RNA cap guanine-N7-methyltransferase. Antivir. Res. 104, 156–164. http://dx.doi.org/10.1016/j.antiviral.2014.02.002.

Van Boheemen, S., Graaf, M. De, Lauber, C., Bestebroer, T.M., Raj, V.S., Zaki, A.M., Osterhaus, A., Haagmans, B.L., Gorbalenya, A., Snijder, E., Fouchier, R., 2012. Genomic characterization of newly discovered coronavirus associated with acute respiratory distress syndrome in humans. mBio 3. http://dx.doi.org/10.1128/mBio.00473-12 e00473–12.

Van Hemert, M.J., Van Den Worm, S.H.E., Knoops, K., Mommaas, A.M., Gorbalenya, A.E., Snijder, E.J., 2008. SARS-coronavirus replication/transcription complexes are membrane-protected and need a host factor for activity in vitro. PLoS Pathog. 4 http://dx.doi.org/10.1371/journal.ppat.1000054.

Varshney, D., Petit, A.-P., Bueren-Calabuig, J.A., Jansen, C., Fletcher, D.A., Peggie, M.,

Weidlich, S., Scullion, P., Pisliakov, A.V., Cowling, V.H., 2016. Molecular basis of RNA guanine-7 methyltransferase (RNMT) activation by RAM. NAR 10, gkw637. http://dx.doi.org/10.1093/NAR/GKW637.

Wu, B., Peisley, A., Richards, C., Yao, H., Zeng, X., Lin, C., Chu, F., Walz, T., Hur, S., 2013. Structural basis for dsRNA recognition, filament formation, and antiviral signal activation by MDA5. Cell 152, 276–289. http://dx.doi.org/10.1016/j.cell.2012.11.048.

Zhang, Y., Wei, Y., Zhang, X., Cai, H., Niewiesk, S., Li, J., 2014. Rational design of human metapneumovirus live attenuated vaccine candidates by inhibiting viral mRNA cap methyltransferase. J. Virol. 88, 11411–11429. http://dx.doi.org/10.1128/jvi.00876-14.

Züst, R., Cervantes-Barragan, L., Habjan, M., Maier, R., Neuman, B.W., Ziebuhr, J., Szretter, K.J., Baker, S.C., Barchet, W., Diamond, M.S., Siddell, S.G., Ludewig, B., Thiel, V., 2011. Ribose 2'-O-methylation provides a molecular signature for the distinction of self and non-self mRNA dependent on the RNA sensor Mda5. Nat. Immunol. 12, 137–143. http://dx.doi.org/10.1038/ni.1979.

Züst, R., Dong, H., Li, X.F., Chang, D.C., Zhang, B., Balakrishnan, T., Toh, Y.X., Jiang, T., Li, S.H., Deng, Y.Q., Ellis, B.R., Ellis, E.M., Poidinger, M., Zolezzi, F., Qin, C.F., Shi, P.Y., Fink, K., 2013. Rational design of a live attenuated Dengue Vaccine: 2'-O-methyltransferase mutants are highly attenuated and immunogenic in mice and macaques. PLoS Pathog. 9, e1003521. http://dx.doi.org/10.1371/journal.ppat.1003521.